Sun-Induced Fluorescence's correlation to carbon-flux increases when raw data is adjusted to account for vegetation biochemistry and structure

Edgard Bontempo [1,2]* and Dalton Valeriano [1] : 1 - Remote Sensing Department, Brazilian National Institute of Space Research (INPE), 2 - Foundation of Science and Application of Space Technology (FUNCATE). Paper # B11Q-2262

Rationale

• Chlorophyll *a* fluorescence or Sun-Induced Fluorescence (SIF, when measured under natural illumination) is emitted by plants at the moment of energy conversion and it relates to the instantaneous level of photosynthesis [1].

• Spectral Vegetation Indices (SVIs), calculated from reflectance at various wavelengths, carry information related to another aspect of plant life: the biomass and its structuration [2, 3, 4, 5, 6].

• SVIs relate to longer term processes than SIF [1,7] and represent longer-term biomass investment into plant survival and growth while SIF represents the current productive status of that biomass.

• Accordingly, reflectance has already been used more than 20 years ago to successfully correct chlorophyll fluorescence output at the leaf level [8].

• Gross Primary Productivity (GPP) can be expressed, according to Monteith [9, 10], as follows:

$$GPP = fAPAR * LUE$$

• Both SIF and SVIs have been successfully used to estimate GPP [11,12].

• These are complementary information sources and, together, present a better picture of reality than in separate.

• Here propose simple combinations of SIF and reflectance based on:

- Monteith's GPP framework [9,10].
- Sellers' two-stream approximation model [3].
- Gitelson's real fluorescence (analogous to SIF_{Yield}) [8].
- and Knyazikhin's Directional Area Scatering Factor (DASF) [6, 13].

• These Spectrally Adjusted SIFs (SASIFs) were tested, along with standard GOME-2 SIF and NIR_V [14], against GPP data from 27 FLUXNET sites of varied Land Cover Classes (LCC) to investigate their relationship to GPP data.

Materials and Methods

All data was tested against the average between daytime and night time partitionings of reference GPP from FLUXNET 2015 dataset sites. All RS data was resampled to a similar grid matching resolution to MODIS MOD13C2. Tested variables are explained in Table 1 below and data used for their calculation was extracted from samples drawn around FLUXNET sites equivalent to one (1px) and four (4px) GOME-2 pixels to alleviate GOME-2 SIF's signal to noise ratio.

We calculated discrepancies between data sampled from 1 and from 4 pixels to subset the data into four groups:
- Full set of 27 sites with unbalanced N (number of samples) from each Land Cover Class (LCC).
- Equal N per LCC, maximum sample.
- Equal N per LCC, only growing season (winter months removed).
- Equal N per LCC, only peak season (3 months per year).

Variable label	Description	Data sources	Quality Flag
SIF_{FR}	Sun-Induced Chlorophyll *a* fluorescence at the far-red wavelenght peak.	GOME-2	*B*
SIF_{FR} * SZA	The product of far-red SIF by the cosine of the Sun's zenith angle.	GOME-2	*B*
$dSIF_{FR}$	A proxy of daily average of SIF_{FR} (daily SIF).	GOME-2	*B*
SIF_R	Sun-Induced Chlorophyll *a* fluorescence at the red wavelenght peak.	GOME-2	*B*
NIR_V	(NDVI - 0.07) * NIR reflectance.	MODIS	*A*
FLUXCOM	A pseudo-control variable, it is the mean of all three estimates of GPP generated from the same FLUXNET dataset as was used in this work.	FLUXCOM RS + Meteo	*A*
$dSIF_{FR}$ * *f*APAR	The product of daily SIF by *f*APAR. *f*APAR = (1.25 * (EVI - 0.1))	GOME-2 and MODIS	*B*
$dSIF_{FR}$ * NDVI	The product of daily SIF by NDVI	GOME-2 and MODIS	*B*
$dSIF_{FR}$ * $NDVI_G$	The product of daily SIF by NDVI (from GOME-2)	GOME-2	*C*
$dSIF_{FR}$ * NIR_V	The product of daily SIF by NIR_V	GOME-2 and MODIS	*B*
$dSIF_{FR}$ * NIR	The product of daily SIF by NIR	GOME-2 and MODIS	*B*
$dSIF_{FR}$: NDVI	The quotient of daily SIF by NDVI - SIF_{Yield}	GOME-2 and MODIS	*B*
$dSIF_{FR}$: $NDVI_G$	The quotient of daily SIF by NDVI (from GOME-2) - SIF_{Yield}	GOME-2	*C*
$dSIF_{FR}$: NDVI * NIR	The quotient of daily SIF by NDVI multiplied by NIR.	GOME-2 and MODIS	*B*

Table 1: Variables tested against FLUXNET GPP. Quality flags refer to: *A*, relatively high spatial resolution and reliable data (i.e., BRDF corrected, validated); *B*, lower spatial resolution, noisy, biased by sensor degradation, and/or radiometrically incompatible; *C*, not recommended for research by authors (no BRDF correction, not validated and subject to sensor degradation bias).

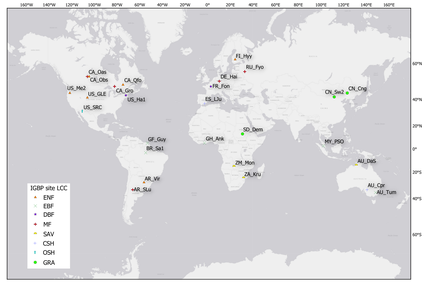

Figure 1: Locations, codes and vegetation types of the FLUXNET 2015 sites used in this study. Land Cover Classes are: ENF - evergreen needleleaf Forest; EBF - evergreen broadleaf forest; DBF - deciduous broadleaf forest; MF - mixed forest; SAV - savannah; CSH - closed shrubland; OSH - open shrubland; GRA - grassland;

Results

The comparison between the two GOME-2 pixel-sized sampling modes showed that GOME-2 data was better correlated to FLUXNET GPP when sampled from 4 pixels instead of from only 1 (results not shown). NIR_V and FLUXCOM were better correlated to FLUXNET GPP when sampled at 1 pixel unit and thus they were employed in further tests.

SASIFs showed improvement in their correlation to GPP when compared to the standard GOME-2 SIF used in their calculation (Fig. 1). SIF_{Yield}-like formulations performed worst in correlations but similarly in Linear-Mixed Models (LMMs). LMM formulation were straightforward but FLUXNET Site, Land Cover Class and Year were included as random factors to constrain models.

Kendall rank correlation tests (Fig. 1), LMM coefficients and RMSE (Fig.2) show that the product of daily SIF_{FR} and *f*APAR had the strongest relationship to FLUXNET GPP, except for our control variable.

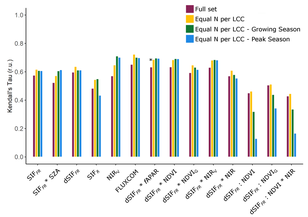

Figure 2: Variable-specific Kendall Rank Correlation Test scores per sample group. Full set N = 1636, Equal N per LCC N = 384, Growing Season N = 224, Peak Season N = 96.

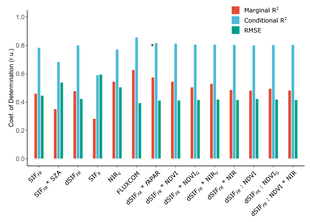

Figure 3: Linear Mixed Model (LMM) metrics. Models are variable specific, with LCC, Site, Month and Year as random variables. R2 is the coefficient of determination; Marginal and Conditional refer to only fixed effects and fixed plus random effects, respectively. RMSE is the root mean squared error of each LMM. N = 384.

Results from Evergreen Needleleaf Forest (ENF) sites show small improvement in SASIF formulations in relation to raw SIF (Figs. 4a and 5a). *f*APAR, NIR, NDVI and NIR_V formulations seem comparable on all sampling groups and, all outperform NIR_V.

Samples from Evergreen Broadleaf Forest (EBF) had the weakest relationships with GPP observed in this study (Figs. 4b and 5b). Interestingly, in this LCC, SIF_{Yield}-like SASIFs performed considerably better than even FLUXCOM data. Most of the data was not significantly correlated to FLUXNET reference GPP (results not shown).

Most variables performed well in Deciduous Broadleaf Forest samples (DBF) and SASIFs were similar to raw SIF (Figs. 4c and 5c).

Mixed Forest (MF) samples and those of open physiognomies Savannah (SAV), Closed Shrublands (CSH) and Open Shrublands (OSH) presented a decreasing pattern of correlation (Figs. 4 and 5, d, e, f and g). While NIR_V showed best results in OSH, SASIFs were equal or superior in MF, SAV and CSH.

Grassland (GRA) results were comparable, if lower, than what was observed in ENF (Figs. 4h and 5h). SIF_R was consistently the least correlated to FLUXNET GPP among all tested variables (with the exception of SAV and CSH sites), and a particularly large difference in performance in GRA data.

In spite of differences in tested data and methods, Kendall τ (tau) scores mostly agreed with LM and LMM metrics (coefficient of determination and RMSE) except in shrubland LCCs (Figs. 4f, 4g, 5f and 5g).

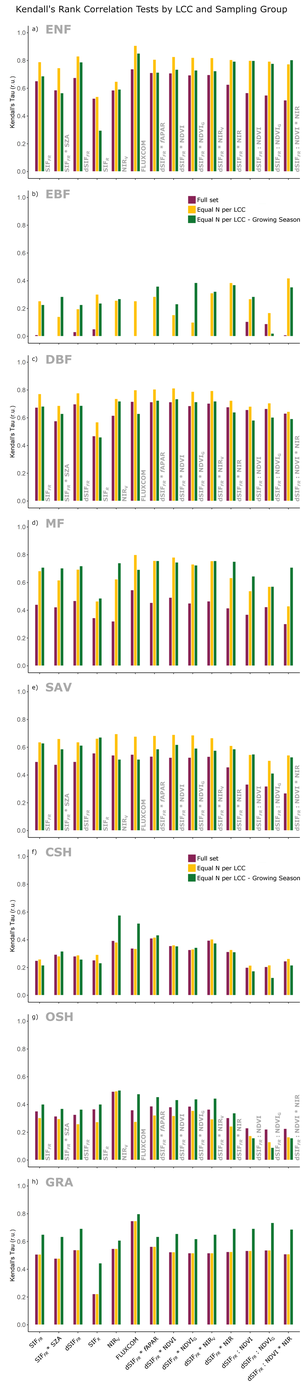

Figure 4: LCC-specific Kendall Rank Correlation Test scores per sample group. Full set N = 1636, Equal N per LCC N = 48, Growing Season N = 28, Peak Season N = 12.

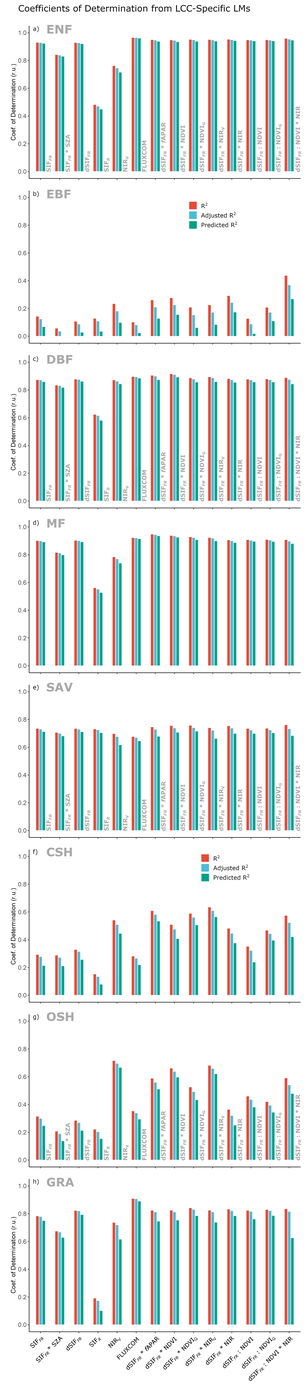

Figure 5: Linear Model (LM) metrics. Models are LCC-specific. Model N = 48 per LCC.

Discussion and Conclusions

Results from LCC-specif tests show that tested variables performance against FLUXNET GPP depends mostly on LCC type and therefore, they are being largely driven by vegetation structure and its effects on radiative transfer.

SIF_{Yield}-like SASIFs (e.g., $dSIF_{FR}$: NDVI and $dSIF_{FR}$: NDVI * NIR), which were assumed to moderate the influences of structure and biochemistry on sampled fluorescence [8], have resulted in a deterioration of the SIF x GPP relationship. This is not surprising if we consider Monteith's original equation [9,10] and the supposed proportionality between SIF and Light Use Efficiency [15, 16, 17].

SIF_R was not well correlated to FLUXNET GPP in most LCC types even if adjusted with reflectance data (results not shown). The observed differences between SIF at red and far-red wavelenght peaks in this study are supported by the known difference in the radiative transfer of fluorescent photons from these regions of the spectra [18] and are expected if one considers the effects of phenological processes as leaf-shedding and chlorophyll degradation on the seasonality of SIF_R reabsorption within the emitting vegetation.

While NIR was shown in previous studies to be almost completely correlated to DASF in an evergreen broadleaved forest [13], it is interesting to see that by itself, it was not as effective to improve the relationship between SIF and GPP as the proxies of chlorophyll content and *f*APAR ($dSIF_{FR}$ * *f*APAR, $dSIF_{FR}$ * NDVI and $dSIF_{FR}$ * NIR_V) employed here, except for Evergreen Broadleaved Forests (EBF).

Furthermore, the lack of pronounced seasonality might be one of the strongest influences on the observed relationship between SIF and GPP at tropical evergreen broadleaved forests. It is perhaps unreasonable to expect that a weak signal such as SIF would be closely related to tower-measured GPP from vegetation with such complex and stratified structure. We suggest that observations in higher spatial resolution, using drone-mounted or tower-mounted sensors for example, should be used to further study SIF x GPP relationship in tropical forests.

The apparent effect of the radiometric incompatibility between the data used here to calculate SASIFs (GOME-2 and MODIS data) is apparently not so great if we consider the differences between SASIFs using NDVI from MODIS and from GOME-2 ($NDVI_G$). Nevertheless, we admit that these tests and their results are inherently imperfect as they are biased by the differences between the sensor from which we got our data.

Despite of the known problems with GOME-2 SIF data (noisy, low resolution, mixed pixel and sensor-degradation bias) [19, 20], we believe that our results support the idea that SIF is an excellent proxy into GPP and that reflectance proxies to plant biochemistry and structure should be used to support the interpretation of chlorophyll fluorescence data.

We suggest that further study is needed and that variables such as the Photochemical Reflectance Index (PRI) [21], already shown to be useful for the investigation of the SIF x GPP relationship [22], should be included. Also better proxies for *f*APAR and chlorophyll content like the recently suggested light absorption coefficient of vegetation [23] can replace some of the terms used here and should also be tested.

References

[1] Govindjee. (1995). Sixty-three years since Kautsky: Chlorophyll a Fluorescence. *Australian Journal of Plant Physiology*, 22, 131–160.
[2] Sellers, P. J., Berry, J. A., Collatz, G. J., Field, C. B., & Hall, F. G. (2003). Canopy reflectance, photosynthesis, and transpiration. III. A reanalysis using improved leaf models and a new canopy integration scheme. *Remote Sensing of Environment*, 42(3), 187–216.
[3] Tucker, C. J. (1979). Red and Photographic Infrared Linear Combinations for Monitoring Vegetation. *Remote Sensing of Environment*, 8(2), 127–150.
[4] Gamon, J. A., Peñuelas, J., & Field, C. B. (1992). A narrow-waveband spectral index that tracks diurnal changes in photosynthetic efficiency. *Remote Sensing of Environment,* 41(1), 35–44.
[5] Huete, A. R., Justice, C., & Leeuwen, W. (1999). *MODIS Vegetation Index (MOD 13): Algorithm Theoretical Basis Document.* Version 3.
[6] Knyazikhin, Y., Mottus, M., Baret, F., Latorre Carmona, P., Kaufmann, R. K., Davis, A. B., et al. (2012). Hyperspectral remote sensing of foliar nitrogen content. *Proceedings of the National Academy of Sciences*, 110(3), E185–E192.
[7] Larcher, W. (2003). *Physiological Plant Ecology* (4th ed.). Springer-Verlag Berlin Heidelberg.
[8] Gitelson, A., Buschmann, C., & Lichtenthaler, H. K. (1998). Leaf chlorophyll fluorescence corrected for re-absorption by means of absorption and reflectance measurements. *Journal of Plant Physiology,* 152(2–3), 283–296.
[9] Monteith, J. L. (1972). Solar Radiation and Productivity in Tropical Ecosystems. *The Journal of Applied Ecology,* 9(3), 747.
[10] Monteith, J. L., & Moss, C. J. (1977). Climate and the Efficiency of Crop Production in Britain [and Discussion]. *Philosophical Transactions of the Royal Society B: Biological Sciences,* 281(980), 277–294.
[11] Guanter, L., Zhang, Y., Jung, M., Joiner, J., Voigt, M., Berry, J. A., et al. (2014, April 8). Global and time-resolved monitoring of crop photosynthesis with chlorophyll fluorescence.
[12] Joiner, J., Yoshida, Y., Zhang, Y., Duveiller, G., Jung, M., Lyapustin, A., et al. (2018). Estimation of terrestrial global gross primary production (GPP) with satellite data-driven models and eddy covariance flux data. *Remote Sensing*, 10(9), 1–38.
[13] Köhler, P., Guanter, L., Kobayashi, H., Walther, S., & Yang, W. (2018). Assessing the potential of sun-induced fluorescence and the canopy scattering coefficient to track large-scale vegetation dynamics in Amazon forests. *Remote Sensing of Environment*, 204, 769–785.
[14] Badgley, G., Field, C. B., & Berry, J. A. (2017). Canopy near-infrared reflectance and terrestrial photosynthesis. *Science Advances*, 3(3).
[15] Ryu, Y., Berry, J. A., & Baldocchi, D. D. (2019). What is global photosynthesis? History, uncertainties and opportunities. *Remote Sensing of Environment*, 223(March), 95–114.
[16] Miao, G., Guan, K., Yang, X., Bernacchi, C. J., Berry, J. A., DeLucia, E. H., et al. (2018). Sun-Induced Chlorophyll Fluorescence, Photosynthesis, and Light Use Efficiency of a Soybean Field from Seasonally Continuous Measurements. Journal of Geophysical Research: Biogeosciences, 123(2), 610–623.
[17] Hilker, T., Coops, N. C., Wulder, M. A., Black, T. A., & Guy, R. D. (2008). The use of remote sensing in light use efficiency based models of gross primary production: A review of current status and future requirements. *Science of The Total Environment*, 404(2–3), 411–423.
[18] Van Wittenberghe, S., Alonso, L., Verrelst, J., Moreno, J., & Samson, R. (2015). Bidirectional sun-induced chlorophyll fluorescence emission is influenced by leaf structure and light scattering properties - A bottom-up approach. *Remote Sensing of Environment,* 158, 169–179.
[19] Joiner, J., Yoshida, Y., Guanter, L., & Middleton, E. M. (2016). New methods for retrieval of chlorophyll red fluorescence from hyper-spectral satellite instruments: simulations and application to GOME-2 and SCIAMACHY. *Atmospheric Measurement Techniques Discussions*, 9(January), 3939–3967.
[20] Joiner, J., Guanter, L., Lindstrot, R., Voigt, M., Vasilkov, A. P., Middleton, E. M., et al. (2013). Global monitoring of terrestrial chlorophyll fluorescence from moderate-spectral-resolution near-infrared satellite measurements: methodology, simulations, and application to GOME-2. *Atmospheric Measurement Techniques,* 6(10), 2803–2823.
[21] Gamon, J. A., Peñuelas, J., & Field, C. B. (1992). A narrow-waveband spectral index that tracks diurnal changes in photosynthetic efficiency. Remote Sensing of Environment, 41(1), 35–44.
[22] Verma, M., Schimel, D., Evans, B., Frankenberg, C., Beringer, J., Drewry, D. T., et al. (2018). Effect of environmental conditions on the relationship between solar-induced fluorescence and gross primary productivity at an OzFlux grassland site. *Journal of Geophysical Research: Biogeosciences*, 122(3), 716–733.
[23] Gitelson, A., Viña, A., Solovchenko, A., Arkebauer, T., & Inoue, Y. (2019). Derivation of canopy light absorption coefficient from reflectance spectra. *Remote Sensing of Environment*, 231(June).

Acknowledgments

Authors would like to thank Lênio Galvão and Anatoly Gitelson for discussion and comments on our initial ideas. We would also like to thank FUNCATE and the Amazon Fund (Fundo Amazônia) for suport and funding.

*Corresponding author's email: edgardbontempo@gmail.com

Please scan the QR-code below for complete contact information.

FUNCATE Fundação de Ciência, Aplicações e Tecnologia Espaciais — INPE — FUNDO AMAZÔNIA